

# Study on mechanical behavior of mono-mineral polycrystalline rock based on 3D intergranular microcracks

Yuichi KARINO

## 1. INTRODUCTION

In previous studies on the fracture of brittle rock, it is mostly assumed that microfractures are initiated and propagate from isolated pre-existing microcracks in rock. Such a crack model cannot be said to represent the crack system in real rock. Moreover, we have few studies on rock fracture, which consider interactions between cracks and failure process after peak stress. To clarify the mechanism for the fracture in rock, it is necessary to perform an analysis by using a rock model having a 3D network of microcracks that influence each other in a complexed manner.

In this study, first, I developed a method for creating on a computer a specimen of polycrystalline rock that has a network of intergranular cracks, assuming that grain boundaries of polycrystalline rock are microcracks (weak planes) in the rock. Second, 3D finite element elastic analysis was performed for the model of the polycrystalline rock in uniaxial compression to estimate the elastic properties and the stress distributions in the intergranular cracks. Finally, fracture analysis was performed for the polycrystalline rock model in uniaxial tension to clarify the influence of the intergranular cracks on the failure process of the polycrystalline rock.

## 2. POLYCRYSTALLINE ROCK MODEL

Fig. 1 shows the surface of the polycrystalline rock model created in this study. The method for creating the polycrystalline rock model is as follows:

- 1) Crystal nuclei that are apart more than a certain distance are generated at random in a specified region.
- 2) Crystals grow from the nuclei simultaneously with the same rate.
- 3) Intergranular cracks (grain boundaries) form between two crystals.
- 4) A cubic specimen model is cut out from the polycrystalline rock model.

In this study, the minimum value for the distance

between crystal nuclei ( $l_m$ ) was introduced and a certain number ( $n$ ) of nuclei were generated in a region. Fig. 2 shows the comparison of the number of vertex in a cross section between the polycrystalline rock model (Fig. 1) and Akiyoshi marble. It can be said that the model reproduces the polycrystalline rock to some degree.

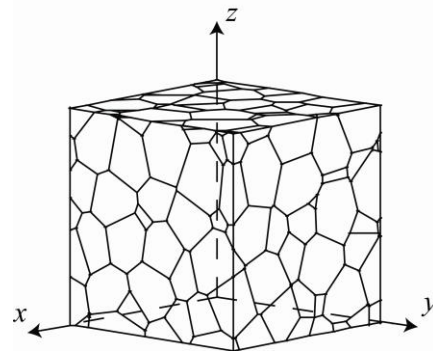


Fig. 1 Polycrystalline model ( $l_m = 20$  mm,  $n = 80$ ).

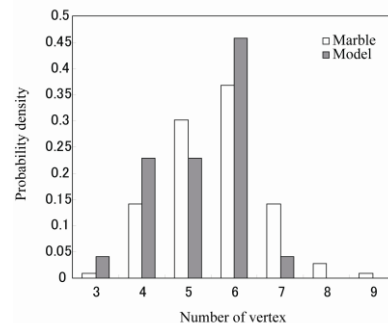


Fig. 2 Comparison of the number of vertex in a cross section.

## 3. ELASTIC ANALYSIS OF THE POLYCRYSTALLINE ROCK MODEL IN UNIAXIAL COMPRESSION

### 3.1 FINITE ELEMENT ANALYSIS

In 3D finite element analysis, crystals were divided into tetrahedral solid elements and crystal planes (intergranular cracks) were divided into triangular joint elements [1]. In the joint element, two planes without thickness were connected to each other with two springs with normal ( $k_n$ ) and shear ( $k_s$ ) stiffnesses.

The elastic analysis was performed in uniaxial compression under the conditions that a uniform displacement in the vertical direction was given to the upper end surface while the lower surface was fixed in the vertical direction. The model used in the elastic analysis was the same as that shown in Fig. 1. By changing the values of  $k_n$  and  $k_s$  for the intergranular cracks, while keeping Young's modulus  $E$  (100 GPa) and Poisson's ratio  $\nu$  (0.2) of the crystals constant, the elastic properties of the model and the stress distributions in the intergranular cracks were estimated.

### 3.2 YOUNG'S MODULUS AND POISSON'S RATIO

Fig. 3 shows the relations between both the effective Young's modulus ( $E_{eff}$ ) and the effective Poisson's ratio ( $\nu_{eff}$ ) of the polycrystalline rock model, the normal stiffness ( $k_n$ ) and the ratio of the shear stiffness to the normal stiffness ( $k_s/k_n$ ). The effective Young's modulus ( $E_{eff}$ ) and the effective Poisson's ratio ( $\nu_{eff}$ ) of the polycrystalline rock model is normalized by Young's modulus ( $E$ ) and Poisson's ratio ( $\nu$ ) of the crystal. The effective Young's modulus ( $E_{eff}$ ) of the polycrystalline rock model is mainly governed by the normal stiffness ( $k_n$ ) and increases with  $k_n$ , while the effective Poisson's ratio ( $\nu_{eff}$ ) of the polycrystalline rock

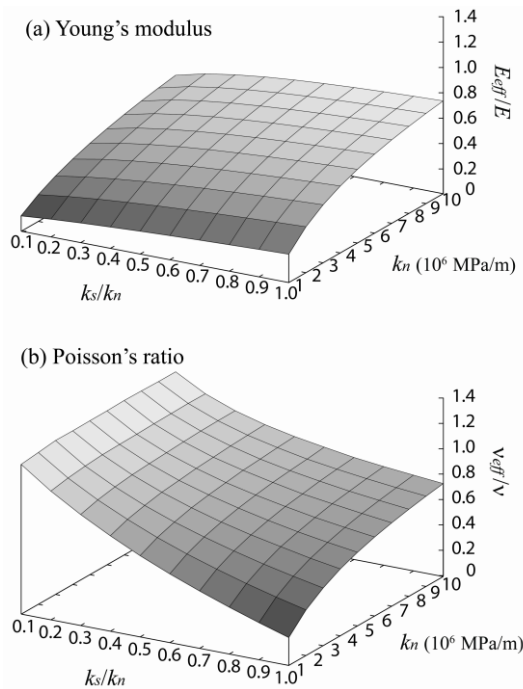


Fig. 3 Effects of  $k_n$  and  $k_s$  on (a)  $E_{eff}/E$  and (b)  $\nu_{eff}/\nu$  of polycrystalline rock model.

model is mainly governed by the ratio of the shear stiffness to the normal stiffness ( $k_s/k_n$ ) and increases with a decrease in  $k_s/k_n$ .

### 3.3 THE DISTRIBUTION OF NORMAL AND SHEAR STRESSES

Fig. 4 shows the relation between the inclination angle ( $\phi$ ) of the intergranular cracks and both normal ( $\sigma_n$ ) and shear ( $\tau$ ) stresses normalized by the magnitude of the axial stress ( $\sigma_z$ ) for  $k_n = 10^6$  MPa/m. The ratios of the shear stiffness to the normal stiffness ( $k_s/k_n$ ) are 1 and 0.1. Tension is positive for the normal stress ( $\sigma_n$ ). Solid circles show the stresses on the cracks that penetrate to the upper and lower end surfaces of the polycrystalline rock model, open squares show those of the cracks that only penetrate to side surfaces, and crosses show those of the other cracks. Solid lines show the stresses in a homogeneous body, as given by

$$\frac{\sigma_n}{|\sigma_z|} = -\frac{1 + \cos 2\phi}{2}, \quad (1)$$

$$\frac{\tau}{|\sigma_z|} = \frac{\sin 2\phi}{2}.$$

As  $k_s/k_n$  decreases, the shear stress ( $\tau$ ) on the intergranular cracks decreases and the normal stress ( $\sigma_n$ ) in the intergranular cracks with a large inclination angle relative to the loading axis

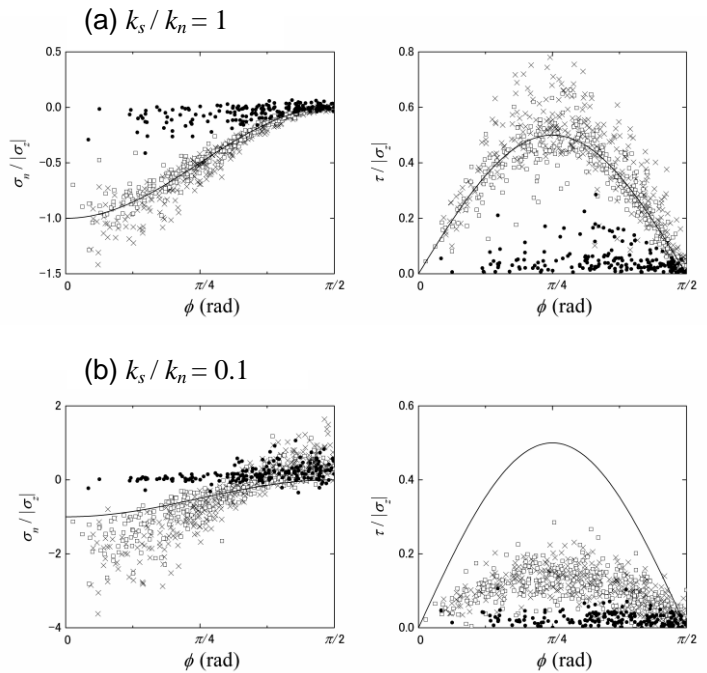


Fig. 4 Relation between  $\phi$  and both  $\sigma_n/|\sigma_z|$  and  $\tau/|\sigma_z|$  for  $k_n = 10^6$  MPa/m, and (a)  $k_s/k_n = 1$  and (b)  $k_s/k_n = 0.1$ .

increases in tension while that with a small inclination angle increases in compression. Thus,  $\sigma_n$  and  $\tau$  deviate more from the values in the homogeneous body as  $k_s/k_n$  decreases. Furthermore, it was found that  $\sigma_n$  and  $\tau$  on the intergranular cracks that penetrate to the upper and lower end surfaces of the polycrystalline rock model (solid circles in Fig. 4), are much smaller than those in other points, since the relative displacements in such intergranular cracks are constrained by the boundary conditions of displacement.

#### 4. FRACTURE BEHAVIOR OF THE POLYCRYSTALLINE ROCK MODEL IN UNIAXIAL TENSION

##### 4.1 METHOD OF ANALYSIS

In this study, the associated flow rule<sup>[2]</sup> in the general theory of plasticity was applied. In order to clarify the influence of the intergranular cracks, it was assumed that the crystals do not fail, but only the boundaries of the crystals will fail.

An extended Coulomb criterion that extends the Coulomb criterion to the tension side was applied, as show in Fig. 5, where the stresses are normalized by the uniaxial tensile strength of the intergranular cracks ( $T_0$ ). Tension is taken to be positive. In the compression side, the peak strength ( $\tau_p$ ) and the residual strength ( $\tau_r$ ) were given by the following equations:

$$\tau_p = c_0 - \mu_0 \sigma_n, \quad (2)$$

$$\tau_r = -\mu_r \sigma_n,$$

where  $c_0$  is the cohesion of the peak strength and  $\mu_0$  and  $\mu_r$  are the frictional coefficients of the peak and residual strengths, respectively. In the tension side, failure criterion was defined by the following equation according to the Brazilian test (broken circle line in Fig. 5):

$$\tau^2 + (\sigma_n + T_0)^2 = 4T_0^2. \quad (3)$$

When the stresses on the intergranular cracks satisfy equations (2) and (3), fracturing starts, and with the progress of failure, the tensile strength ( $T$ ) changes from  $T_0$  to 0, the shear strength ( $\tau$ ) changes from  $\tau_p$  to  $\tau_r$  and the cohesion ( $c$ ) changes from  $c_0$  to 0. When the tensile strength of an intergranular fracture is  $T$ , the failure condition in tension is given by

$$\tau^2 + (\sigma_n + T)^2 = 4T^2, \quad (4)$$

and that in compression is given by

$$\tau = c - \mu \sigma_n, \quad (5)$$

where  $T$ ,  $c$  and  $\mu$  are tensile strength, cohesion, and frictional coefficient in the failure process. Frictional coefficient ( $\mu$ ) is assumed to decrease linearly with the tensile strength from  $\mu_0$  to  $\mu_r$ . The cohesion ( $c$ ) is expressed by a function of  $T$  to smoothly connect equation (4) with equation (5). The relation between the normal and shear stresses ( $\sigma_{nb}$ ,  $\tau_b$ ) at the boundary between tension and compression is shown by solid line in Fig. 5. When an intergranular crack is fractured in tension, this is called tensile failure and when it is fractured in compression, this is called shear failure.

Tension-shear softening law was assumed for the intergranular fracture, as was given by the following equation:

$$T = T_0 \exp\left(-\gamma \frac{k_n}{T_0} \delta_{ep}\right), \quad (6)$$

where  $\gamma$  is a coefficient that expresses the speed of failure progress and  $\delta_{ep}$  is an equivalent permanent displacement determined from the permanent normal ( $\delta_{np}$ ) and shear displacements ( $\delta_{sp}$ ), as given by

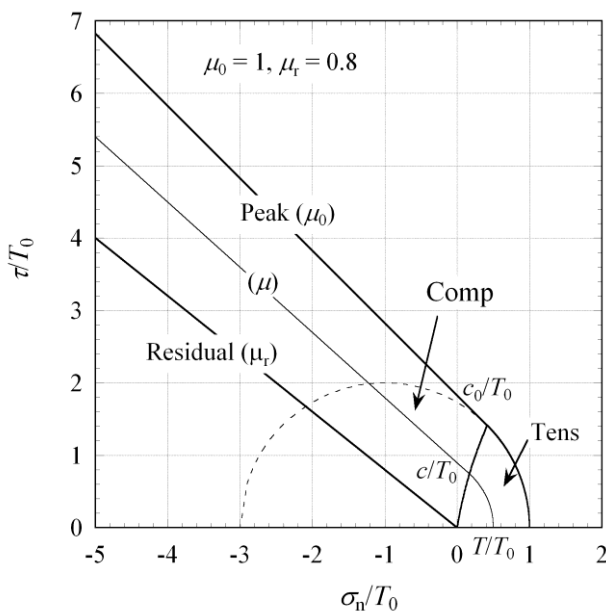


Fig. 5 Failure criterion.

$$\delta_{ep} = \sqrt{\delta_{np}^2 + \delta_{sp}^2}. \quad (7)$$

## 4.2 THE CONDITIONS OF ANALYSIS

For the 3D finite element fracture analysis, polycrystalline rock models were created with  $l_m = 50$  mm and  $n = 10$ . Table 1 shows the mechanical properties used in the simulation to simulate hard rocks.

Table 1 Mechanical properties used in the simulation.

$E$ (GPa)	$\nu$	$k_n$ (MPa/m)	$k_s$ (MPa/m)	$\mu_0$	$\mu_r$	$T_0$ (MPa)
100	0.2	$5.0 \times 10^6$	$2.5 \times 10^6$	1.0	1.0	1.0

## 4.3 RESULTS

### 4.3.1 FAILURE PROCESS IN UNIAXIAL TENSION

Fig. 6 shows a typical stress-strain curve and a change in the number of failure mode during failure process ( $\gamma = 0.1$ ). When paying attention to the change in the number of failure mode, first of all, tensile failure occurs before the peak and unloading begins to occur around the peak. After the peak, tensile failure modes decrease to be transformed by shear failure modes.

Such fracture behavior can be explained by the following mechanism. In the beginning, tensile failures occur for the intergranular cracks with the normal direction near the loading axis. Then, the failure mode of the intergranular fractures with tensile mode changes to unloading when the fracture cannot be a part of the main fracture. As the

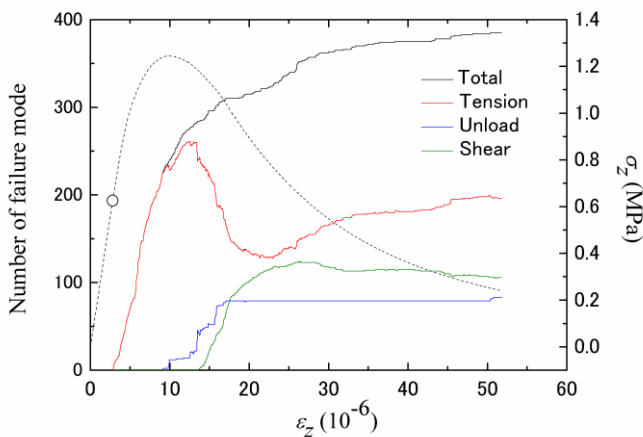


Fig. 6 Stress-strain curves and change in the number of failure mode.

failure progress, tensile fractures with the normal direction that is deviated from the loading axis change their failure mode to shear failure in order to connect fractures to form a main fracture, and a main fracture surface gradually forms.

### 4.3.2 INFLUENCE OF TENSION-SHEAR SOFTENING LAW

Fig. 7 shows stress-strain curves when the coefficient  $\gamma$  in the tension-shear softening law is changed. As  $\gamma$  increases, the stress and strain at peak decrease and stress drop after peak becomes rapid, since the number of intergranular fracture decreases as  $\gamma$  increases.

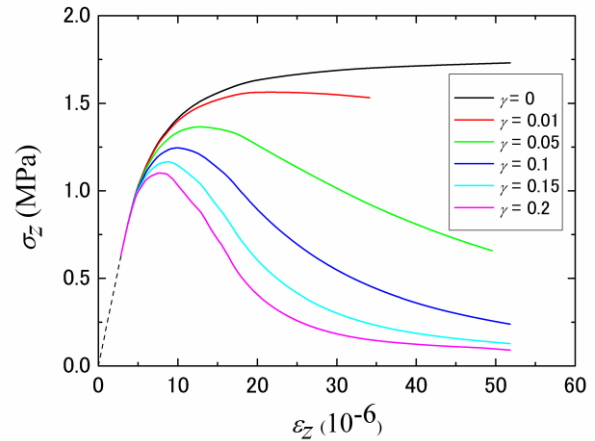


Fig. 7 Stress-strain curves for  $\gamma = 0, 0.01, 0.05, 0.1, 0.15,$  and  $0.2$ .

## 5. CONCLUSION

In this study, first, I developed a method for creating a polycrystalline rock model and showed that the method can reproduce a real polycrystalline rock. Second, elastic analysis in uniaxial compression was performed for the model and the elastic properties of the model and the stress distribution in the intergranular cracks were estimated. Finally, fracture analysis was performed in uniaxial tension and the influences of the intergranular cracks on the failure process of the polycrystalline rock were clarified.

## REFERENCES

- [1] K. Matsuki et al: Int. J. Rock Mech. Min. Sci., **46** (2009), 31-50.
- [2] O.C.Zienkiewicz: *The Finite Element Method (3<sup>rd</sup> edition)*, McGraw Hill, 1979, pp. 450-471.